Electron-impact ionization of atomic ions in the W isonuclear sequence

S. D. Loch, J. A. Ludlow, and M. S. Pindzola
Department of Physics, Auburn University, Auburn, Alabama 36849, USA

A. D. Whiteford
Department of Physics, University of Strathclyde, Glasgow, Scotland

D. C. Griffin
Department of Physics, Rollins College, Winter Park, Florida, USA
(Received 7 September 2005; published 22 November 2005)

Electron-impact ionization cross sections for all atomic ions in the W isonuclear sequence are calculated using a variety of theoretical methods. For the direct ionization process, a semirelativistic configuration-average distorted-wave method is used for low to moderately charged ions, while a fully relativistic subconfiguration-average distorted-wave method is used for highly charged ions. For the indirect ionization process of excitation autoionization, a semirelativistic configuration-average distorted-wave method is used for the bulk of the transitions, but a semirelativistic level-resolved distorted-wave method is used for selective strong transitions that may straddle the ionization threshold. For moderately charged ions it is important to include radiation damping of the excitation-autoionization process through explicit calculation of autoionization branching ratios. Checks are made on the theoretical predictions by comparison with available crossed-beams experimental measurements, which only exist for low stages of ionization. The ionization cross sections for the entire W isonuclear sequence are converted to temperature-dependent rate coefficients and put in a collisional-radiative format that should prove useful in modeling laboratory plasmas that contain W impurities.

DOI: 10.1103/PhysRevA.72.052716 PACS number(s): 34.50.Fa

I. INTRODUCTION

With the future construction of the International Tokamak Experimental Reactor (ITER) in Cadarache, France, most existing tokamak experiments are investigating design issues and diagnostic applications relevant for ITER operation. The design plans for ITER call for certain plasma facing components in the divertor region to be made out of tungsten, to withstand the high heat load on those surfaces. There are also plans to use heavy species, like hafnium and tungsten, for diagnostic purposes, such as wall erosion markers. In light of these plans, there have been numerous experiments using tungsten in current tokamak devices, such as the ASDEX-Upgrade [1]. These experiments, and future ITER operation, require a significant amount of atomic data for tungsten emission modeling. The data required involve mainly electron-ion collisions, and include excitation, recombination (radiative and dielectronic), and ionization processes.

Experimental measurements for the electron-impact ionization cross sections for W ions have been confined to the lower charge states. The crossed-beams technique has been used to measure ionization cross sections for W^+ [2] and for all W^{q+} ions in charge states $q=1-10$ [3]. Experimental measurements [2,3] for W^+ are found to be 40% lower than semirelativistic distorted-wave calculations [4] for the direct ionization cross section alone. However, for W^{4+}, W^{5+}, and W^{6+} reasonable agreement is found between theory [5] and experiment [2], where excitation-autoionization contributions are found to be strong for each ion. We are not aware of other *ab initio* theoretical work on the ionization of tungsten ions.

In this paper, we calculate electron-impact ionization cross sections for all atomic ions in the W isonuclear sequence using a variety of theoretical and computational methods. Of specific interest in this paper is the trend along the isonuclear sequence of various physical effects. For example, when is excitation autoionization important, when does radiative damping quench the excitation-autoionization cross section, and at what point does one need to use a fully relativistic treatment in the ionization cross-section calculations? Our ionization cross sections for all W ions are converted to temperature-dependent rate coefficients and put in a collisional-radiative format that should prove useful in modeling laboratory plasmas that contain W impurities. In the following section we describe the semirelativistic and fully relativistic distorted-wave methods used to calculate the direct ionization and excitation-autoionization processes, in Sec. III we present selected examples of W ionization cross sections to illustrate physical effects, and in Sec. IV we discuss the overall accuracy of the present calculations and what remains to be done in future work.

II. THEORY

In the independent processes approximation the total ionization cross section is given by

$$\sigma_{total} = \sigma_{direct} + \sum_j \sigma^j_{excit} B^a_j, \tag{1}$$

where σ_{direct} is the direct ionization cross section, σ_{excit} is the excitation cross section of an inner-shell electron to an autoionizing level j, and B^a_j is the branching ratio for autoionization from the level j, given by

$$B_j^a = \frac{\sum_m A_a(j \to m)}{\sum_m A_a(j \to m) + \sum_n A_r(j \to n)}, \tag{2}$$

where A_a is the autoionizing rate and A_r is the radiative rate. We neglect the resonant excitation followed by sequential double autoionization process, since it is computationally involved, even at the configuration-average distorted-wave level, it is generally a small fraction of the total ionization cross section, and it is confined to a small energy range below the upper excitation-autoionization thresholds [6].

A. Direct ionization

For low to moderately charged atomic ions, the direct ionization cross section may be calculated using a semirelativistic configuration-average distorted-wave method [7]. The most general transition between configurations is of the form

$$(nl)^w k_i l_i \to (nl)^{w-1} k_e l_e k_f l_f, \tag{3}$$

where w is the occupation number, and nl, $k_i l_i$, $k_e l_e$, and $k_f l_f$ are the quantum numbers of the bound electron and the incident, ejected, and final continuum electrons. The configuration-average direct ionization cross section is given by

$$\sigma_{direct} = \int_0^{E/2} d\epsilon_e \frac{32w}{k_i^3 k_e k_f} \sum_{l_i,l_e,l_f} (2l_i+1)(2l_e+1)(2l_f+1) \times (M_d + M_e - M_x), \tag{4}$$

where the linear momentum $k=\sqrt{2\epsilon}$, the total energy $E=\epsilon_{nl}+\epsilon_i=\epsilon_e+\epsilon_f$, and the continuum normalization is chosen as 1 times a sine function. The direct, exchange, and interference scattering terms M are products of standard algebraic nj symbols and radial integrals which include static electrodynamic interactions. The energies and bound orbitals needed to evaluate the cross section of Eq. (4) are calculated in the Hartree-Fock relativistic (HFR) approximation [10], which includes the mass velocity and Darwin corrections within modified HF differential equations. The continuum radial orbitals are obtained by solving a single-channel Schrodinger equation, which also includes the mass-velocity and Darwin corrections, where the distorting potential is constructed from HFR bound orbitals.

For highly charged atomic ions, the direct ionization cross section may be calculated using a fully relativistic subconfiguration-average distorted-wave method [8,9]. The most general transition between subconfigurations is of the form

$$(nlj)^w p_i l_i j_i \to (nlj)^{w-1} p_e l_e j_e p_f l_f j_f, \tag{5}$$

where nlj, $p_i l_i j_i$, $p_e l_e j_e$, and $p_f l_f j_f$ are now the quantum numbers of the bound electron and the incident, ejected, and final continuum electrons. The subconfiguration-average direct ionization cross section is given by

$$\sigma_{direct} = \int_0^{E/2} d\epsilon_e \frac{16w}{p_i^3 p_e p_f} \sum_{l_i,l_e,l_f} \sum_{j_i,j_e,j_f} (2j_i+1)(2j_e+1)(2j_f+1) \times (\bar{M}_d + \bar{M}_e - \bar{M}_x), \tag{6}$$

where the linear momentum $p=\sqrt{2\epsilon+\epsilon^2/c^2}$ and the continuum normalization is $\sqrt{1+\epsilon/2c^2}$ times a sine function. The direct, exchange, and interference scattering terms $\bar{M}$ are products of standard algebraic nj symbols and radial integrals which include static, magnetic, and retardation electrodynamic interactions. The energies and bound orbitals needed to evaluate the cross sections of Eq. (6) are calculated in the Dirac-Fock (DF) approximation [11]. The continuum radial orbitals are obtained by solving a single channel two-component Dirac equation, where the distorting potential is constructed from DF bound orbitals.

B. Inner-shell excitation

For low to moderately charged atomic ions, the inner-shell excitation cross section may be calculated using a semirelativistic configuration-average distorted-wave method [7]. The most general transition between configurations is of the form

$$(n_1 l_1)^{w_1+1} (n_2 l_2)^{w_2-1} k_i l_i \to (n_1 l_1)^{w_1} (n_2 l_2)^{w_2} k_f l_f, \tag{7}$$

where $n_1 l_1$ and $n_2 l_2$ are quantum numbers of the bound electrons and $k_i l_i$ and $k_f l_f$ are quantum numbers of the initial and final continuum electrons. The configuration-average excitation cross section is given by

$$\sigma_{excit} = \frac{8\pi}{k_i^3 k_f} (w_1+1)(4l_2+3-w_2) \times \sum_{l_i,l_f} (2l_i+1)(2l_f+1)(M_d + M_e - M_x). \tag{8}$$

The energies and orbitals needed to evaluate Eq. (8) are again calculated in the HFR approximation.

The inner-shell excitation cross section may also be calculated using a semirelativistic level-resolved multiconfiguration distorted-wave method [12]. The most general transition between levels is of the form

$$(\alpha_i J_i) k_i l_i j_i J \to (\alpha_f J_f) k_f l_f j_f J, \tag{9}$$

where J_i is the total angular momentum for the target bound state, α_i represents all other quantum numbers needed to specify the intermediate-coupled target bound state, J is the total angular momentum of the electron-ion system, and $k_i l_i j_i$ and $k_f l_f j_f$ are the quantum numbers of the incident and final continuum electrons. The level-resolved excitation cross section is given by

$$\sigma_{exc}(i \to f) = \frac{4\pi}{k_i^3 k_f} \frac{1}{2(2J_i+1)} \sum_{l_i j_i} \sum_{l_f j_f} \sum_J (2J+1) \times |T(\alpha_i J_i k_i l_i j_i J \to \alpha_f J_f k_f l_f j_f J)|^2, \tag{10}$$

where the T matrix for a given J and parity is related to the K matrix by the expression

$$T = -\frac{2iK}{1 - iK}, \tag{11}$$

and the K matrix is given by

$$K^J_{fi} = -\langle \alpha_f J_f k_f l_f j_f | H - E | \alpha_i J_i k_i l_i j_i J \rangle, \tag{12}$$

where H is the semirelativistic Hamiltonian for the collision system. The energies and orbitals needed to evaluate Eqs. (10)–(12) are again calculated in the HFR approximation.

C. Branching ratios for autoionization

For low to moderately charged atomic ions, the radiative and autoionization rates needed to evaluate the branching ratio for autoionization of Eq. (2) may be calculated using a semirelativistic configuration-average distorted-wave method [7]. The most general autoionizing transitions between configurations are of the form

$$(n_1 l_1)^{w_1} (n_2 l_2)^{w_2} (n_3 l_3)^{w_3} \rightarrow (n_1 l_1)^{w_1+1} (n_2 l_2)^{w_2-1} (n_3 l_3)^{w_3-1} k_e l_e, \tag{13}$$

or

$$(n_1 l_1)^{w_1} (n_2 l_2)^{w_2} \rightarrow (n_1 l_1)^{w_1+1} (n_2 l_2)^{w_2-2} k_e l_e, \tag{14}$$

where $n_1 l_1$, $n_2 l_2$, and $n_3 l_3$ are quantum numbers of the bound electrons and $k_e l_e$ are the quantum numbers of the ejected continuum electron. The configuration-average autoionization rate for the first transition type is given by

$$A_a = \frac{w_2 w_3 (4l_1 + 2 - w_1)}{k_e} (4l_e + 2)(M_d + M_x - M_c), \tag{15}$$

with similar expressions for configuration-average radiative rates and autoionization rates of the second transition type [7]. The energies and orbitals needed to evaluate the rate of Eq. (15) are again calculated in the HFR approximation.

The autoionization branching ratios may also be calculated using a semirelativistic level-resolved multiconfiguration distorted-wave method, as found in the Cowan atomic structure package [10]. The bound and continuum orbitals are again calculated in the HFR approximation. We note that for highly charged atomic ions, the indirect ionization process of excitation autoionization makes very little contribution since the autoionization branching ratios are essentially zero.

III. RESULTS

Semirelativistic configuration-average distorted-wave (CADW) calculations for both direct and indirect ionization contributions have been performed along the entire W isonuclear sequence. These have been supplemented by more detailed semirelativistic level to level distorted-wave (LLDW) calculations for excitation-autoionization contributions of particular ion stages and by fully relativistic subconfiguration-average distorted-wave (SCADW) calculations for direct ionization contributions of highly charged ion stages. In Table I we list the ground configurations for the entire W isonuclear sequence and the direct ionization cross section contributions by subshell. The ground configurations are taken from theoretical energy-level tables [13]. The majority of the direct ionizations result in a single ionization, however, there are some which lie above the double ionization threshold. Indirect excitation-autoionization contributions are determined from the same set of listed subshells, minus the outer subshell. Excitations begin with inner subshell transitions to the first unfilled outer subshell, followed by transitions to all allowed outer subshells with $n \leqslant 8$ and $l \leqslant 3$. A contribution whose excitation threshold energy is below that of the single ionization threshold is discarded, since its states cannot autoionize.

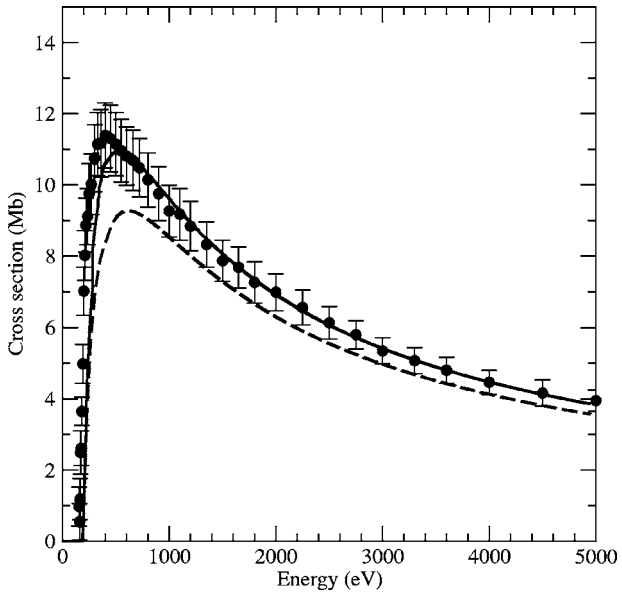

FIG. 1. Electron-impact ionization cross section for W^{9+}. Dashed curve: CADW calculations for direct ionization; solid curve: CADW calculations for direct and indirect ionization; solid circles: experimental measurements [3] (1.0 Mb = 1.0×10^{-18} cm^2).

For near-neutrals, distorted-wave theory performs poorly and tends to overestimate experiment, however, by W^{4+}, W^{5+}, and W^{6+}, distorted-wave theory [5] is in reasonable agreement with experimental measurements [3]. For these low ion stages the autoionization branching ratios of Eq. (2) are very close to 1. As an illustration of a typical low ion stage, we compare distorted-wave theory and experiment for W^{9+} in Fig. 1, where both direct ionization and indirect excitation autoionization have been included. W^{9+} has the ground configuration $[\mathrm{Kr}]4d^{10}4f^{13}5s^2 5p^4$. Direct ionization from the $5p$, $5s$, $4f$, and $4d$ subshells and excitation autoionization from the $5s$, $4f$, and $4d$ subshells were calculated in a CADW approximation. The indirect ionization makes a relatively small contribution, however, it is important in obtaining good agreement with experiment [3]. Above W^{10+} experimental data are not available, however, the good agreement between theory and experiment by W^{4+} gives confidence in the accuracy of the distorted-wave results.

From W^{11+} to W^{27+} excitation-autoionization contributions remain relatively small. For these ion stages the total ionization cross section is generally dominated by direct ionization from the outer $4d$ and $4f$ subshells. The autoionization branching ratios are still close to 1 for these ion stages.

TABLE I. Ground-state configurations for W ions and direct ionization contributions by subshell.

Ion stage	Configuration	Direct subshell contributions
0	$[Xe]4f^{14}5d^46s^2$	$6s,5d,5p$
1	$[Xe]4f^{14}5d^46s$	$6s,5d,5p$
2	$[Xe]4f^{14}5d^4$	$5d,5p,5s$
3	$[Xe]4f^{14}5d^3$	$5d,5p,5s$
4	$[Xe]4f^{14}5d^2$	$5d,5p,5s$
5	$[Xe]4f^{14}5d$	$5d,5p,5s$
6	$[Xe]4f^{14}$	$5p,5s,4f,4d$
7	$[Xe]4f^{13}$	$5p,5s,4f,4d$
8	$[Kr]4d^{10}4f^{13}5s^25p^5$	$5p,5s,4f,4d$
9	$[Kr]4d^{10}4f^{13}5s^25p^4$	$5p,5s,4f,4d$
10	$[Kr]4d^{10}4f^{13}5s^25p^3$	$5p,5s,4f,4d$
11	$[Kr]4d^{10}4f^{13}5s^25p^2$	$5p,5s,4f,4d$
12	$[Kr]4d^{10}4f^{13}5s^25p$	$5p,5s,4f,4d$
13	$[Kr]4d^{10}4f^{13}5s^2$	$5s,4f,4d$
14	$[Kr]4d^{10}4f^{12}5s^2$	$5s,4f,4d$
15	$[Kr]4d^{10}4f^{11}5s^2$	$5s,4f,4d$
16	$[Kr]4d^{10}4f^{11}5s$	$5s,4f,4d$
17	$[Kr]4d^{10}4f^{11}$	$4f,4d,4p$
18	$[Kr]4d^{10}4f^{10}$	$4f,4d,4p$
19	$[Kr]4d^{10}4f^9$	$4f,4d,4p$
20	$[Kr]4d^{10}4f^8$	$4f,4d,4p$
21	$[Kr]4d^{10}4f^7$	$4f,4d,4p$
22	$[Kr]4d^{10}4f^6$	$4f,4d,4p$
23	$[Kr]4d^{10}4f^5$	$4f,4d,4p$
24	$[Kr]4d^{10}4f^4$	$4f,4d,4p$
25	$[Kr]4d^{10}4f^3$	$4f,4d,4p$
26	$[Kr]4d^{10}4f^2$	$4f,4d,4p$
27	$[Kr]4d^{10}4f$	$4f,4d,4p$
28	$[Kr]4d^{10}$	$4d,4p,4s,3d$
29	$[Kr]4d^9$	$4d,4p,4s,3d$
30	$[Kr]4d^8$	$4d,4p,4s,3d$
31	$[Kr]4d^7$	$4d,4p,4s,3d$
32	$[Kr]4d^6$	$4d,4p,4s,3d$
33	$[Kr]4d^5$	$4d,4p,4s,3d$
34	$[Kr]4d^4$	$4d,4p,4s,3d$
35	$[Kr]4d^3$	$4d,4p,4s,3d$
36	$[Kr]4d^2$	$4d,4p,4s,3d$
37	$[Kr]4d$	$4d,4p,4s,3d$
38	$[Ar]3d^{10}4s^24p^6$	$4p,4s,3d$
39	$[Ar]3d^{10}4s^24p^5$	$4p,4s,3d$
40	$[Ar]3d^{10}4s^24p^4$	$4p,4s,3d$
41	$[Ar]3d^{10}4s^24p^3$	$4p,4s,3d$
42	$[Ar]3d^{10}4s^24p^2$	$4p,4s,3d$
43	$[Ar]3d^{10}4s^24p$	$4p,4s,3d$
44	$[Ar]3d^{10}4s^2$	$4s,3d,3p$
45	$[Ar]3d^{10}4s$	$4s,3d,3p$
46	$[Ar]3d^{10}$	$3d,3p,3s$
47	$[Ar]3d^9$	$3d,3p,3s$
48	$[Ar]3d^8$	$3d,3p,3s$
49	$[Ar]3d^7$	$3d,3p,3s$
50	$[Ar]3d^6$	$3d,3p,3s$
51	$[Ar]3d^5$	$3d,3p,3s$
52	$[Ar]3d^4$	$3d,3p,3s$
53	$[Ar]3d^3$	$3d,3p,3s$
54	$[Ar]3d^2$	$3d,3p,3s$
55	$[Ar]3d$	$3d,3p,3s$
56	$[Ne]3s^23p^6$	$3p,3s,2p$
57	$[Ne]3s^23p^5$	$3p,3s,2p$
58	$[Ne]3s^23p^4$	$3p,3s,2p$
59	$[Ne]3s^23p^3$	$3p,3s,2p$
60	$[Ne]3s^23p^2$	$3p,3s,2p$
61	$[Ne]3s^23p$	$3p,3s,2p$
62	$[Ne]3s^2$	$3s,2p,2s$
63	$[Ne]3s$	$3s,2p,2s$
64	$1s^22s^22p^6$	$2p,2s$
65	$1s^22s^22p^5$	$2p,2s$
66	$1s^22s^22p^4$	$2p,2s$
67	$1s^22s^22p^3$	$2p,2s$
68	$1s^22s^22p^2$	$2p,2s$
69	$1s^22s^22p$	$2p,2s$
70	$1s^22s^2$	$2s$
71	$1s^22s$	$2s$
72	$1s^2$	$1s$
73	$1s$	$1s$

We show direct and indirect ionization cross sections for W^{22+} in Fig. 2. W^{22+} has the ground configuration $[Kr]4d^{10}4f^6$. Direct ionization from the $4f$, $4d$, and $4p$ subshells and excitation-autoionization from the $4d$ and $4p$ subshells were calculated in a CADW approximation. Excitation autoionization is about a third of the direct cross section.

From W^{28+} through to W^{45+}, CADW calculations with autoionization branching ratios set to 1 find that excitation-autoionization cross sections become equal in magnitude to the direct ionization cross section. However, for these moderately ionized stages, radiative decay may become higher than autoionization, and the branching ratio is then considerably less than 1. This reduces the excitation autoionization contribution. For these ion stages, configuration-average distorted-wave ionization calculations were carried out that included configuration-average autoionization branching ratios. For W^{28+} these branching ratios are close to one, but reduce significantly by W^{45+}

To check the accuracy of the configuration-average distorted-wave calculations of excitation-autoionization contributions, we also carried out level to level distorted-wave calculations. This is illustrated for W^{45+} in Figs. 3 and 4.

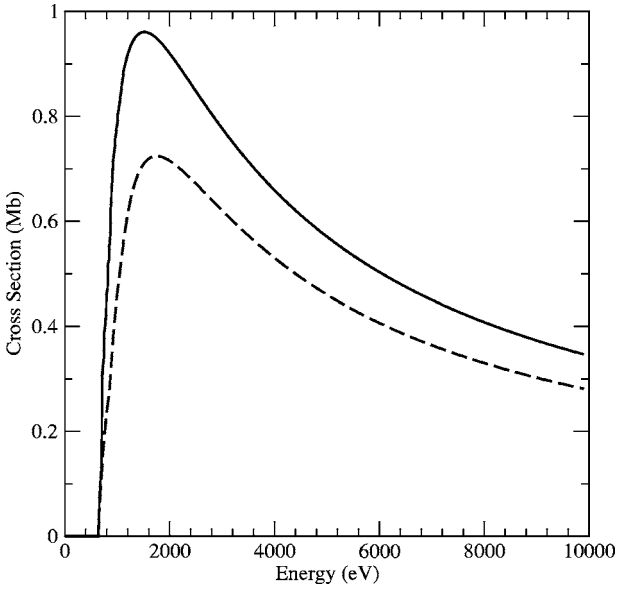

FIG. 2. Electron-impact ionization cross section for W^{22+}. Dashed curve: CADW calculations for direct ionization; solid curve: CADW calculations for direct and indirect ionization (1.0 Mb=1.0×10^{-18} cm^2).

W^{45+} has the ground configuration [Ar]$3d^{10}4s$. The presence of a single $4s$ electron above a filled $3d$ subshell leads to large $3d\rightarrow nl$ excitation cross sections. However, it is found that the inclusion of autoionization branching considerably reduces the contribution of excitation-autoionization, seen in both the CADW calculations of Fig. 3 and the LLDW calculations of Fig. 4.

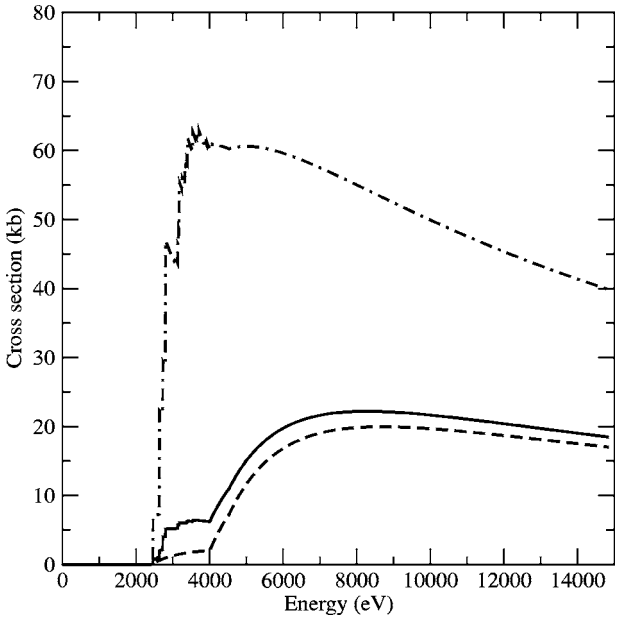

FIG. 3. Electron-impact ionization cross section for W^{45+}. Dashed curve: CADW calculations for direct ionization; dot-dashed curve: CADW calculations for direct and indirect ionization with unit branching; solid curve: CADW calculations for direct and indirect ionization with full branching (1.0 kb=1.0×10^{-21} cm^2).

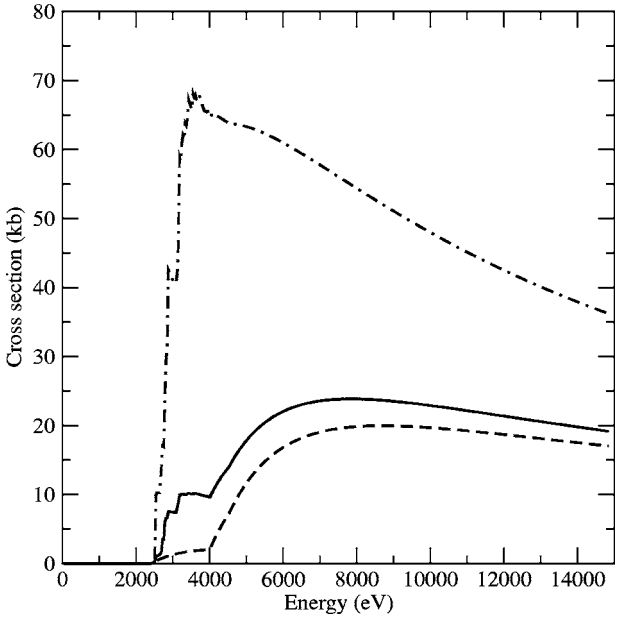

FIG. 4. Electron-impact ionization cross section for W^{45+}. Dashed curve: CADW calculations for direct ionization; dot-dashed curve: CADW calculations for direct ionization and LLDW calculations for indirect ionization with unit branching; solid curve: CADW calculations for direct ionization and LLDW calculations for indirect ionization with full branching (1.0 kb=1.0×10^{-21} cm^2).

From W^{46+} to W^{55+} excitation-autoionization contributions again remain relatively small. The ionization cross section is dominated by direct ionization from the outer $3d$ subshell. As we move to the highly ionized stages of W^{56+} and beyond, the normally important excitation-autoionization contribution is almost completely eliminated by radiation damping. The total ionization cross section is approximately equal to the direct cross section. This is illustrated for W^{63+} in Fig. 5, where CADW calculations are presented. For lighter elements than W, the Na-like ion stage generally has large excitation-autoionization contributions [14]. However, as can be seen in Fig. 5, with the inclusion of radiation damping through the autoionization branching ratio, the excitation-autoionization contributions are almost wiped out.

For the highest ion stages, relativistic effects become increasingly important and it is important to use a fully relativistic treatment. Fully relativistic SCADW and semirelativistic CADW calculations are compared for Ne-like W^{64+} in Fig. 6. The CADW results lie about 20% below the SCADW calculations. Fully relativistic SCADW and semirelativistic CADW calculations are compared for He-like W^{72+} in Fig. 7. By W^{72+}, relativistic effects dominate, leading to a factor of 2–3 difference between the CADW and SCADW results.

Thus the electron-impact ionization cross sections for the entire W isonuclear sequence are calculated using the following approximations. For ion stages $W-W^{27+}$: CADW calculations for direct ionization and for excitation with unit autoionization branching ratios; for ion stages $W^{28+}-W^{45+}$: CADW calculations for direct ionization and for excitation and autoionization branching ratios; for ion stages $W^{46+}-W^{63+}$: CADW calculations for direct ionization only;

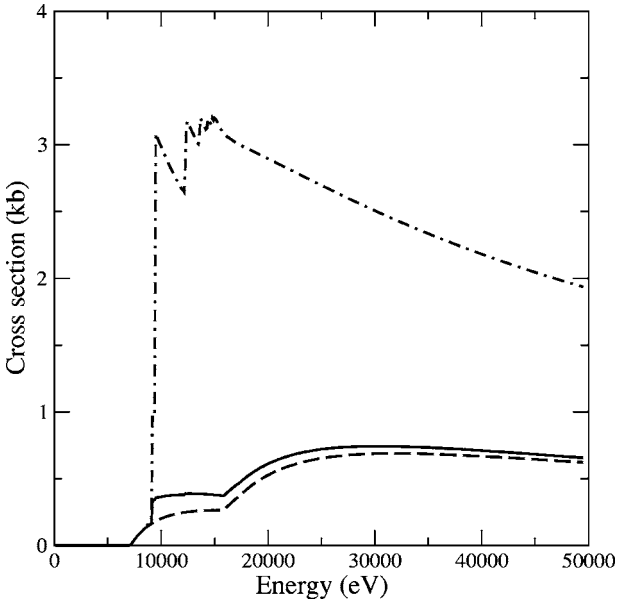

FIG. 5. Electron-impact ionization cross section for W^{63+}. Dashed curve: CADW calculations for direct ionization; dot-dashed curve: CADW calculations for direct and indirect ionization with unit branching; solid curve: CADW calculations for direct and indirect ionization with full branching (1.0 kb=1.0×10^{-21} cm^2).

and for ion stages W^{64+}–W^{73+}: SCADW calculations for direct ionization only. These ionization cross sections for the entire W isonuclear sequence have been converted to temperature-dependent Maxwellian-averaged rate coefficients and put in a collisional-radiative format dictated by the JET-Strathclyde Atomic Data and Analysis Structure (ADAS) project [15]. Electron-impact ionization Maxwellian-averaged rate coefficients are now available in electronic format at the ORNL Controlled Fusion Atomic Data Center (CFADC) [16]. Total temperature-dependent rate coefficients are available for the Fe [17], Ni [18], Kr [19], and now W isonuclear sequences; level-resolved temperature-dependent rate coefficients are available for all ionization stages of the light elements Be, B, C, N, O, and Ne [20]; and temperature- and density-dependent generalized collisional-radiative rate-coefficients are available for the Li and Be isonuclear sequences.

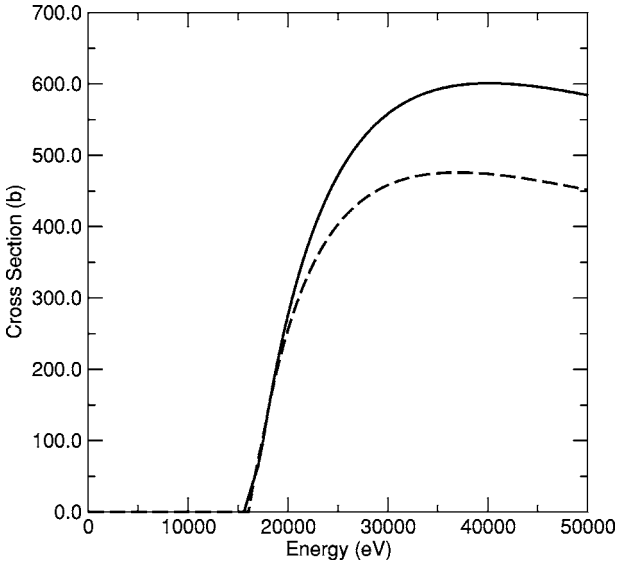

FIG. 6. Electron-impact ionization cross section for W^{64+}. Dashed curve: CADW calculations for direct ionization; solid curve: SCADW calculations for direct ionization (1.0 b=1.0×10^{-24} cm^2).

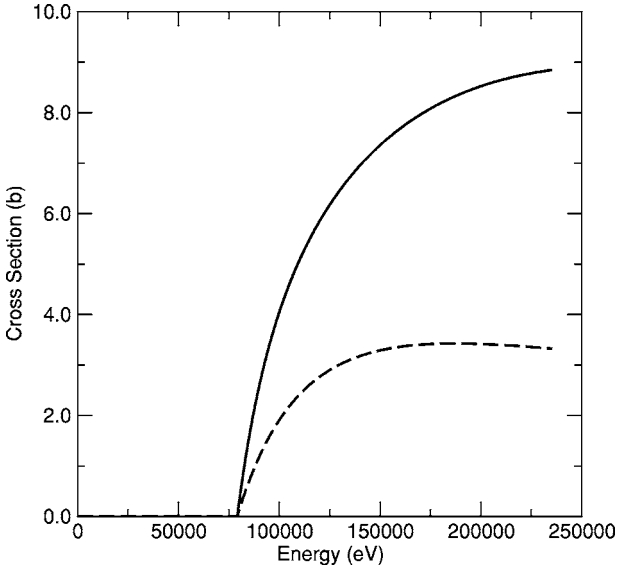

FIG. 7. Electron-impact ionization cross section for W^{72+}. Dashed curve: CADW calculations for direct ionization; solid curve: SCADW calculations for direct ionization (1.0 b=1.0×10^{-24} cm^2).

IV. SUMMARY

In this paper, the electron impact ionization of tungsten has been studied along its entire isonuclear sequence. For near-neutrals, distorted-wave theory performs poorly, however, by W^{4+}, distorted-wave theory and experiment are in reasonable agreement when both direct and indirect ionization contributions are included in the calculations. As we move higher in ion stage, radiation damping becomes important, acting to reduce the indirect excitation-autoionization contributions. This was illustrated for W^{45+}, where the inclusion of radiation damping was seen to considerably reduce the large excitation-autoionization contributions. For higher ion stages, excitation autoionization is almost wiped out by radiation damping. Finally, the importance of using a fully relativistic treatment of direct ionization was demonstrated for the highest ion stages in the W isonuclear sequence.

Based on our calculations for electron-impact ionization along the entire W isonuclear sequence, we have assembled a database of Maxwellian-averaged rate coefficients for use in laboratory plasma modeling. Various approximations were used in the electron-impact ionization calculations to obtain a complete database. For near-neutral ion stages, our theoretical predictions for direct plus indirect ionization are

generally larger than experimental crossed-beam measurements. Unfortunately, the use of experimental measurements for low ion stages is complicated by the unknown fraction of ground and metastable states present in the ion beam. In the future much work remains to be done. At a minimum, we plan to extend our ionization calculations to include excited configurations that may contain sizeable numbers of metastable levels. We also plan to revise our present database with nonperturbative calculations of direct ionization in low ion stages and with further LLDW calculations of excitation-autoionization contributions through to the highest ion stages.

ACKNOWLEDGMENTS

This work was supported in part by grants from the U.S. Department of Energy. Computational work was carried out at the National Energy Research Scientific Computing Center in Oakland, California, and at the National Center for Computational Sciences in Oak Ridge, Tennessee.

[1] R. Neu, R. Dux, A. Kallenbach, T. Putterich, M. Balden, J. C. Fuchs, A. Herrmann, C. F. Maggi, M. O'Mullane, R. Pugno, I. Radivojevic, V. Rohde, A. C. C. Sips, W. Suttrop, A. Whiteford, and the ASDEX Upgrade team, Nucl. Fusion **45**, 209 (2005).

[2] R. G. Montague and M. F. A. Harrison, J. Phys. B **17**, 2707 (1984).

[3] M. Stenke, K. Aichele, D. Hathiramani, G. Hofmann, M. Steidl, R. Volpel, and E. Salzborn, J. Phys. B **28**, 2711 (1995).

[4] M. S. Pindzola and D. C. Griffin, Phys. Rev. A **46**, 2486 (1992).

[5] M. S. Pindzola and D. C. Griffin, Phys. Rev. A **56**, 1654 (1997).

[6] N. R. Badnell and M. S. Pindzola, Phys. Rev. A **47**, 2937 (1993).

[7] M. S. Pindzola, D. C. Griffin, and C. Bottcher, in *Atomic Processes in Electron-Ion and Ion-Ion Collisions*, Vol. 145 of NATO Advanced Studies Institute, Series B: Physics, edited by F. Brouillard (Plenum, New York, 1986), p. 75.

[8] M. S. Pindzola and M. J. Buie, Phys. Rev. A **37**, 3232 (1988).

[9] M. S. Pindzola, D. L. Moores, and D. C. Griffin, Phys. Rev. A **40**, 4941 (1989).

[10] R. D. Cowan, *The Theory of Atomic Structure and Spectra* (University of California Press, Berkeley, 1981).

[11] I. P. Grant, B. J. McKenzie, P. H. Norrington, D. F. Mayers, and N. C. Pyper, Comput. Phys. Commun. **21**, 207 (1980).

[12] D. C. Griffin, C. Bottcher, and M. S. Pindzola, Phys. Rev. A **25**, 1374 (1982).

[13] T. H. Carlson, C. W. Nestor, N. Wassermann, and J. D. McDowell, At. Data **2**, 63 (1970).

[14] M. S. Pindzola, D. M. Mitnik, J. A. Shaw, D. C. Griffin, N. R. Badnell, H. P. Summers, and D. R. Schultz, Phys. Scr. **57**, 514 (1998).

[15] H. P. Summers and M. G. O'Mullane, in *Nuclear Fusion Research*, edited by R. E. H. Clark and D. H. Reiter (Springer, New York, 2005), p. 399.

[16] http://www-cfadc.phy.ornl.gov

[17] M. S. Pindzola, D. C. Griffin, C. Bottcher, S. M. Younger, and H. T. Hunter, Nucl. Fusion Special Suppl. **1**, 21 (1987).

[18] M. S. Pindzola, D. C. Griffin, C. Bottcher, M. J. Buie, and D. C. Gregory, Phys. Scr. **T37**, 35 (1991).

[19] S. D. Loch, M. S. Pindzola, C. P. Ballance, D. C. Griffin, D. M. Mitnik, N. R. Badnell, M. G. O'Mullane, H. P. Summers, and A. D. Whiteford, Phys. Rev. A **66**, 052708 (2002).

[20] M. S. Pindzola, D. C. Griffin, N. R. Badnell, and H. P. Summers, Nucl. Fusion Suppl. **6**, 117 (1996).